

## FACTORS INFLUENCING THE PREPARATION OF ULTRA-FINE ZrB<sub>2</sub> POWDERS VIA CARBOTHERMAL REDUCTION

Y. F. WANG, F. ZHANG, Y. B. DUAN, K. J. WANG, W. J. ZHANG, J. HU\*

*Department of Materials Science and Engineering, Kunming University of Science and Technology, Kunming 650093, China*

The effect of different molar ratio between Zr<sup>4+</sup> and citric acid, different pH values, temperatures and dispersant (polyethylene glycol) contents on amorphous precursor of zirconium diboride (ZrB<sub>2</sub>) and synthesized powders were investigated. The fourier transform infrared spectroscopy showed that the optimal condition of complexation is Zr<sup>4+</sup>/citric acid molar ratio of 2 and pH value is 1. Field emission scanning electron microscopy (FESEM) showed that synthesized powders exhibited near-spherical morphology with a low temperature (50 °C) with the increase of temperature, ZrB<sub>2</sub> powders proceeded with the growth process which was complied with the Ostwald ripening model and the Ostwald-Freundlich equation. Transmission electron microscopy (TEM) showed, besides the dispersing function, polyethylene glycol could also facilitate crystal grains to reunite, and result in the ordered arrangement of crystal grains, the synthesized powders with excellent homogeneity and dispersity, especially with the polyethylene glycol content of 2 wt.%. The following particle size distribution measured by laser particle size analyzer had also provided clear evidence for this.

(Received May 4, 2017; Accepted July 28, 2017)

*Keywords:* Sol-gel; Carbothermal reduction; Amorphous precursor; Zirconium diboride powders; Ostwald ripening model

### 1. Introduction

As an important member of ultra-high-temperature ceramics, ZrB<sub>2</sub> ceramics have great potential for application in the field of high-temperature structural material [1-3], because of its unique chemical stability and excellent physical properties, such as high melting temperature, low density, high strength, high thermal conductivity, resistance to high-temperature oxidation, ablation and thermal shock [4-9]. In previous studies, it has been found that high purity fine ZrB<sub>2</sub> powders as raw materials could enhance the mechanical properties and increase the driving force for sintering [10-11]. Therefore, in the last decade, there has been an increasing focus on the production of ceramic powder with ultrafine or nano-scale particles and nano-grained sintered particles. Exceptional properties such as excellent sinterability and improved mechanical properties of the formed nano-grained particles are the motivation for this focus [12-13].

Presently, ZrB<sub>2</sub> powders could be synthesized by these methods of solid-state reaction, electrochemical, mechanical alloying and self-propagating high-temperature synthesis. However, these methods either require a high temperature or a long production period, besides, the powders synthesized from these methods also have a relatively larger particle size and poor sinterability. There is thereby an urgent need but it is still a significant challenge to develop ideal ZrB<sub>2</sub> powders. For purpose of fabricating ultra-fine ZrB<sub>2</sub> powders with ideal size and high purity, many researchers have adopted sol-gel method which is high intimacy at atomic-scale or molecular-scale. In our previous study, ZrB<sub>2</sub> powders with particle size range of 0.2~0.6µm and specific surface area of 88.14 m<sup>2</sup>/g had been synthesized successfully from inorganic-organic hybrid precursors via carbothermal reduction [14]. However, the effect of some factors on the synthesis and growth process of ZrB<sub>2</sub> powders remains obscure now and needs further investigation.

---

\* Corresponding author: kmust651111@126.com



resulted in the transformation of B-OH into B-O-C bond. In addition, there existed several obvious peaks formed by hydrolysis of  $Zr^{4+}$  complex anions at low wavenumbers (i.e.  $645\text{cm}^{-1}$  and  $537\text{cm}^{-1}$ ). From FTIR spectrum as shown in Fig.1, the characteristic absorption peaks of  $819\text{cm}^{-1}$ ,  $1033\text{cm}^{-1}$ ,  $1188\text{cm}^{-1}$  were assigned to Zr-O-Zr, Zr-O-C and Zr-O-C-B bond, respectively [18]. With the proceeding of hydrolysis and condensation reaction, Zr-O-Zr and Zr-O-C-B networks were formed in the sol. Compared to single Zr-O-Zr network structure, the sol consisting of Zr-O-Zr and Zr-O-C-B networks became more stable and uniform in our research [19]. By contrast, the whole characteristic vibrating peaks gets maximum intensity when R is 2. Therefore, the optimal ratio of  $Zr^{4+}$ /citric acid was experimentally determined as 2 in our research.

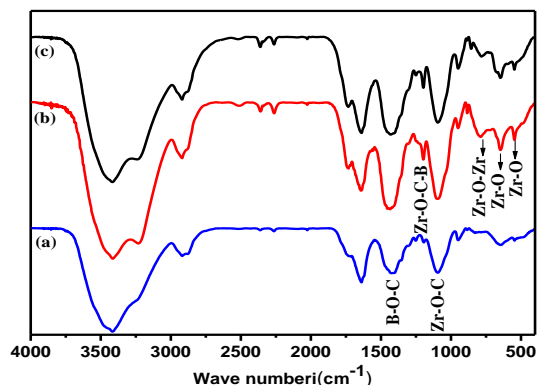


Fig. 1. Infrared analysis of the precursor with different molar ratio between  $Zr^{4+}$  and citric acid  
(a)  $R=3$ ; (b)  $R=2$ ; (c)  $R=1$

Fig. 2 shows FTIR spectra of the precursor powders with different pH values. For reference, the infrared analysis of citric acid was also included (Fig. 2(d)). In experimental process, with gradual addition of ammonium hydroxide, there firstly generated milky precipitation and then turned to be colorless transparent. In the early stage of the reaction, after adding certain amount of ammonia-water equivalent to citric acid, then continued to increase the pH value of reaction system, there would form coordinate band between  $Zr^{4+}$  and citrate ions generated from completely acidolysis of citric acid. Moreover, this coordination compound displays electrically neutral and thus generated colloidal precipitate. When the reaction system turns to be alkaline, there formed the combination of  $Zr^{4+}$  and a certain amount of hydroxyl, this coordination compound become negatively charged accordingly and thus colloidal precipitate dissolved to be transparent. There existed obvious characteristic absorption peak at  $1720\text{cm}^{-1}$ , which was assigned to the C=O (carbonyl group) antisymmetric stretching vibration of  $-\text{COOH}$  (fig. 2(d)). Close to the characteristic absorption peak of C=O, There existed another characteristic peak at  $1667\text{cm}^{-1}$  originated from the carbonyl group of  $\text{COO}^-$  complexing with  $Zr^{4+}$  [20]. It could be observed clearly that these characteristic peaks were weakened gradually with the increase of pH value, it reaches the strongest when pH value is 1 (Fig. 2(a)). Nonetheless, when the pH value is 8, these characteristic peaks of Zr-O and Zr-O-Zr became weaker and even disappeared (Fig. 2(c)), namely that the alkaline condition goes against the complexation reaction of  $Zr^{4+}$  and citric acid. Taken together, it demonstrated that the pH value is crucial as it exerts significant influence on the stability of sol, especially in the acidic reaction system. Therefore, the optimal pH value is 1 in this synthesis reaction system.

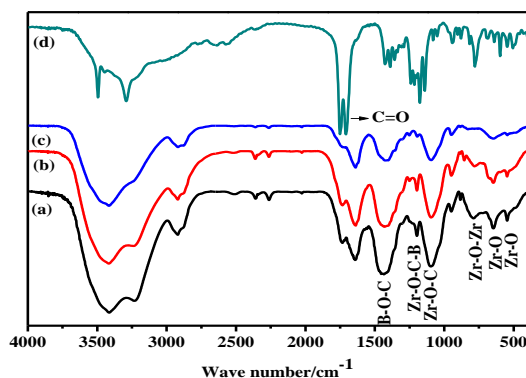


Fig. 2. Infrared analysis of the precursor with different pH  
 (a) pH=1 ; (b) pH=4 ; (c) pH=8

FE-SEM micrographs of  $ZrB_2$  powders obtained with different temperatures provide insight into the particle morphology in Fig.3. Trends in the product morphology are clearly observable. The particle size of  $ZrB_2$  increased from about 150-430nm (Fig.3(a)) for the lowest sol-gel temperature, to submicron values for the highest sol-gel temperature (Fig.3(c)). When the temperature was low (50°C), it can nucleate rapidly and generally avoid secondary nucleating, Therefore,  $ZrB_2$  powders with a narrow size range exhibited near-spherical morphology (Fig.3(a)). Upon heating to a relatively high temperature (60°C),  $ZrB_2$  particles, which exhibited irregular morphology, gradually increased and distributed nonuniformly. Meanwhile, there existed some smaller particles (Fig.3(b)). As temperature increased to 70°C, there were much more smaller  $ZrB_2$  particles deposited onto the surface of big  $ZrB_2$  particles (Fig.3(c)). According to the Ostwald Ripening model, this thermodynamically-driven spontaneous process occurs because larger particles are energetically favored than smaller particles [21]. This stems from the fact that molecules on the surface of a particle are energetically less stable than the ones in the interior. As the system tries to lower its overall energy, as shown in Fig.4, molecules on the surface of a small  $ZrB_2$  particle will tend to detach from the particle and diffuse into the solution. When all small  $ZrB_2$  particles do this, it increases the concentration of free molecules in solution. When the free molecules in solution are supersaturated, the free molecules have a tendency to condense on the surface of larger  $ZrB_2$  particles. Therefore, all small  $ZrB_2$  particles shrink while larger  $ZrB_2$  particles grow, and overall the average size will increase.

According to Ostwald-Freundlich equation:

$$S = S_0 \exp\left(\frac{2\gamma_{SL}V_m}{R_g T_r}\right) \quad (2)$$

Where  $S$  is the solubility of small particles with a radius of  $r$ ;  $S_0$  is the constant;  $\gamma_{SL}$  is the molar ratio of solid phase materials;  $R_g$  is the ideal gas constant;  $T_r$  is the temperature. Thus, with the increase of temperature, the solubility of small  $ZrB_2$  particles decreases and they redeposit onto the surface of those big particles (Fig.3(c)). Increase in temperature also weakens the intermolecular interactions in liquids so that the viscosity of liquids decreases, this leads to molecular collision happening more frequently and the probability of particles agglomeration increase. Finally, size of  $ZrB_2$  particles increase with high-temperature pyrogenation [22]. Besides, for hydrolysis reaction belonging to endothermic reaction, the increase of temperature also contributes to hydrolysis reaction, increase crosslinking points, accelerate the aging of colloidal particles in the solution and ultimately make the size of colloidal particles increase [23].

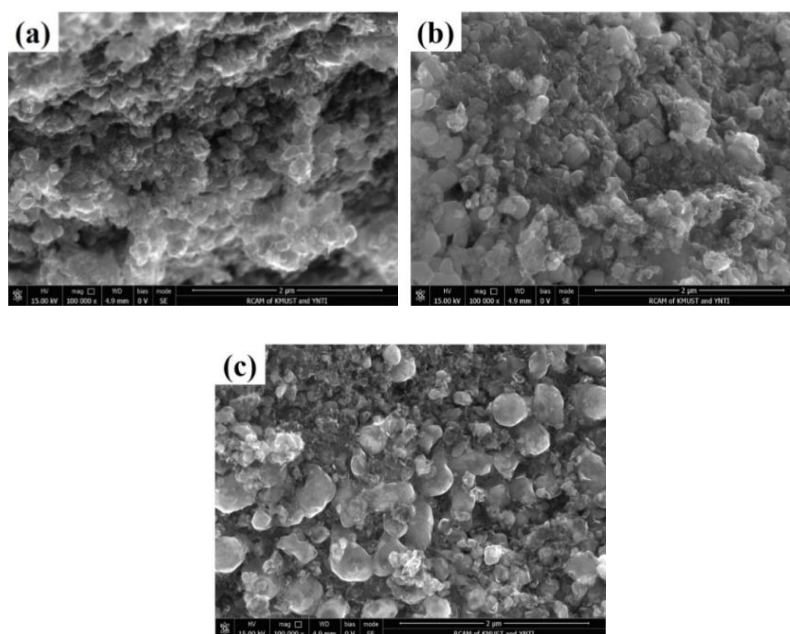


Fig. 3. FE-SEM images of  $ZrB_2$  powders with different temperatures.  
(a) 50 °C; (b) 60 °C; (c) 70 °C

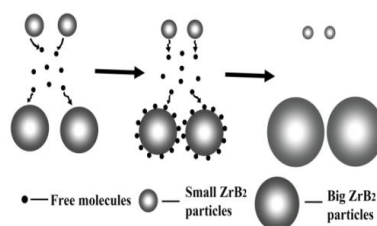


Fig. 4. Schematic of  $ZrB_2$  particles Ostwald ripening

Fig.5 shows TEM images of  $ZrB_2$  powders with different polyethylene glycol contents. Without polyethylene glycol,  $ZrB_2$  grains aggregated heavily and arranged irregularly (Fig. 5(a)). When polyethylene glycol content was 1 wt.%,  $ZrB_2$  grains' dispersion had been improved and it displayed some of regularity (Fig. 5(b)). For polyethylene glycol additions up to 2 wt.%, these  $ZrB_2$  grains dispersed better overall, especially that individual grain could be observed clearly (Fig. 5(c)). Addition of polyethylene glycol content higher than 2 wt.% resulted in that  $ZrB_2$  grains aggregated heavily again, reunited and finally formed big  $ZrB_2$  particles. Moreover, small grains contained in individual  $ZrB_2$  particles showed the similar arrangement orientation (Fig. 5(d)).

Polyethylene glycol in the product phase is located as a coating on the formed  $ZrB_2$  grains' surface. The formed  $ZrB_2$  grains are surrounded by polyethylene glycol and are embedded in the round shaped formation of polyethylene glycol, which plays a key role in the refining of the  $ZrB_2$  particle size by keeping apart the  $ZrB_2$  grains. Addition of polyethylene glycol not only prevents the growth of colloidal grains, but also makes colloids crosslink in order for "bridging effect" of citric acid and polyethylene glycol. Finally, it forms chain or annulus structure in the sol-gel system, which could contribute to the colloid stability [24, 25]. Under the influence of surface hydroxyl groups of polyethylene glycol, small grains coated with excessive amount of polyethylene glycol reunite and form small particle clusters, subsequently these small  $ZrB_2$  particle clusters collide and permeate with each other to form big particle clusters, just as we observed in Fig.5(d). Taken together, polyethylene glycol can not only coat the surface of particles to achieve dispersion effect, but also can be a "guide" to the cross linking of the clusters in the sol.

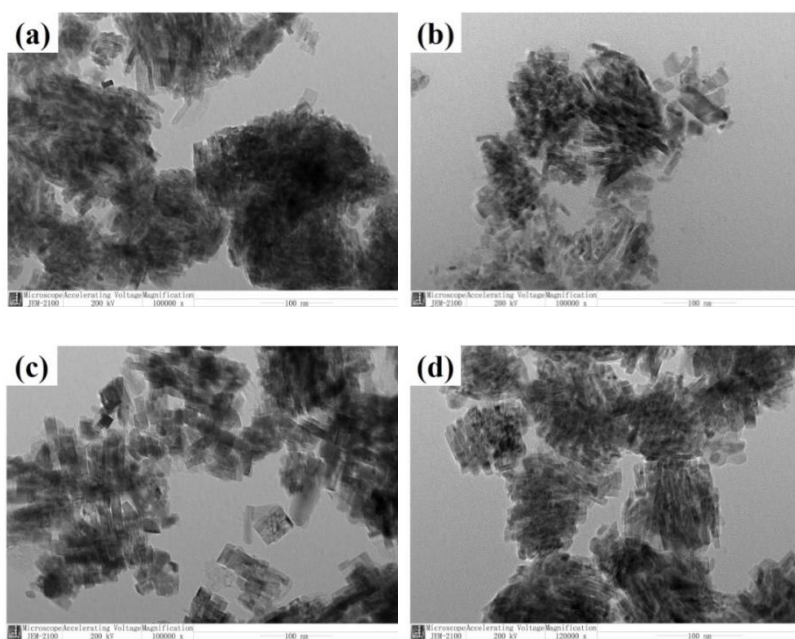


Fig. 5. TEM images of the products with different polyethylene glycol contents. (a) no added, (b) 1 wt.%, (c) 2 wt.%, (d) 3 wt.%.

Fig. 6 shows the patterns of particles size distribution of  $ZrB_2$  powders obtained with 0 and 2 wt.% polyethylene glycol contents. Table.1 shows the characteristic size values of  $ZrB_2$  particles. With the addition of 2 wt.% polyethylene glycol content, The average particle size of  $ZrB_2$  decreased from 260nm to 190nm and the distribution range of  $ZrB_2$  particles size narrowed further (Fig. 6, Table.1). It proves that proper addition of polyethylene glycol plays a key role in the refining of the  $ZrB_2$  particle size by keeping apart the  $ZrB_2$  grains.

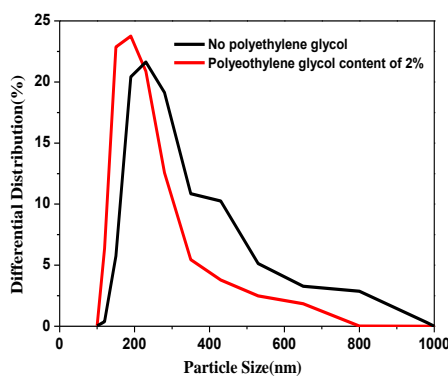


Fig. 6. The patterns of differential distribution of  $ZrB_2$  powders. (a)  $r=2, pH=4, T=50\text{ }^\circ\text{C}$ ; (b)  $r=2, pH=4, T=50\text{ }^\circ\text{C}, c=2\%$

Table 1. Characteristic values of  $ZrB_2$  powders particle size

Content/nm	D50	D10	D25	D75	D90
(a)	260	160	180	340	450
(b)	190	120	140	230	290

#### 4. Conclusions

Effects of the molar ratio of  $Zr^{4+}$  to citric acid, sol-gel temperature, pH value and content of polyethylene glycol on  $ZrB_2$  powders synthesized by carbothermal reduction were investigated. It was discovered that, the optimum condition of complexation reaction was  $Zr^{4+}$ /citric acid molar ratio of 2 and pH value of 1. When the temperature was low ( $50^\circ C$ ),  $ZrB_2$  powders exhibited near-spherical morphology and dispersed well, the increase of temperature resulted in the growth of  $ZrB_2$  powders which process complied with the Ostwald ripening model and the Ostwald-Freundlich equation. Besides the disperse function, polyethylene glycol can also guide sol grains to reunite, this resulted in the ordered arrangement of crystal particles and synthesized powders with good homogeneity and dispersity, especially with polyethylene glycol content of 2 wt.%.

#### Acknowledgement

This work was financially supported by the National Natural Science Foundation of China (No.U1037601).

#### References

- [1] Q. N. Nguyen, E. J. Opila, R. C. Robinson, *J. Electrochem. Soc.*, **151**, B558 (2004).
- [2] S. R. Levine, E. J. Opila, M. C. Halbig, et al., *J. Eur. Ceram. Soc.*, **22**, 2757 (2002).
- [3] S. C. Zhang, G. E. Hilmas, W. G. Fahrenholtz, *J. Eur. Ceram. Soc.*, **31**, 893 (2001).
- [4] X. T. Shen, K. Z. Li, H. J. Li, et al., *Carbon*, **48**, 344, (2010).
- [5] E. L. Corral, L.S. Walker, *J. Eur. Ceram. Soc.*, **30**, 2357 (2010).
- [6] W.G. Fahrenholtz, G.E. Hilmas, I.G. Talmy, et al. *J. Am. Ceram. Soc.* **90**, 1347 (2007).
- [7] A.L. Chamberlain, W.G. Fahrenholtz, G.E. Hilmas, *J. Eur. Ceram. Soc.* **29**, 3401 (2009).
- [8] S.Q. Gao, *J. Eur. Ceram. Soc.* **29**, 995 (2009).
- [9] R. Mitra, S. Upendar, M. Mallik, et al. *J. Eur. Ceram. Soc.* **31**, 1811 (2011).
- [10] W. G. Fahrenholtz, G. E. Hilmas, S. C. Zhang, S. Zhu, *J. Am. Ceram. Soc.* **91**, 1398 (2008).
- [11] A. Rezaie, W. G. Fahrenholtz, G. E. Hilmas, *J. Mater. Sci.*, **42**, 2735 (2007).
- [12] A. K. Khanra, M. M. Godkhindi, L. C. Pathak, *Mater. Sci. Eng. A*. 281 (2004).
- [13] G. Cao, *Nanostructures and Nanomaterials*. Imperial College Press, London, 2004, pp. 357-358.
- [14] Wang Bai-na, Duan Yun-biao, Hu Jin. *J. Key Engineering Materials*. **607**, 54 (2016).
- [15] Y. J. Yan, Z. R. Huang, S. M. Dong, D. L. Jiang, *J. Am. Ceram. Soc.* **89**(11), 3585 (2006).
- [16] K. Kustin, R. Pizer., *J. Am. Ceram. Soc.*, **91**, 317 (1969).
- [17] L Babcock. R. Pizer, *J. Inorg. Chem.* **19**, 56 (1980).
- [18] Y.T. Li, X.Y. Tao, W.F. Qiu, *J. Beijing Uni. Chem. Technol.*, **37**, 79 (2010).
- [19] Huiming Ji, Ming Yang, Minmin Li, Guangyi Ji, Hongna Fan, Xiaohong Sun, *J. Advanced Powder Technology*. **25**, 910 (2014).
- [20] Y. L. Chen, Z. B. Huang, H. M. Ji, et al., *J. Chemical Industry and Engineering* **30**, 7 (2013).

- [21] Ratke, Lorenz, Voorhees, Peter W. Growth and Coarsening: Ostwald Ripening in Material Processing. Springer. pp. 117-118.
- [22] X. L. Liu, W. Q. Zhang, P. H. Liang, J. Acta Photonica Sinica **28**(6), 558 (1999).
- [23] J. C. G. Pereira, C. R. Gatlow, G. D. Rice, J. Phys Chem A, 106 (2002).
- [24] Sun Jinhong, Zhang Bin, Fan Wenzhi, et al., J. Chinese Journal of Materials Research. **13**, 301 (1999).
- [25] J. M. Tang, C. S. Zhu, H. P. Xia, et al. Chinese Journal of Materials Research. **12**, 79 (1998).